FLOWS IN COMPOUNDS THAT MODEL CRYSTAL GROWTH IN BRIDGMAN FURNACES

Second Semi-Annual Report on
NASA Grant NAG-1-627

by
Patrick G. Barber
Professor and Director of Chemistry
Longwood College, Farmville, Virginia 23901

25 September 1988

Enclosed is a paper submitted to the Journal of Crystal Growth on the work done under NASA Research Grant NAG-1-627.

MODELING MELT-SOLID INTERFACES IN BRIDGMAN GROWTH

Patrick G. BARBER
Longwood College, Farmville, Virginia 23901
and
Robert F. BERRY, William J. DEBNAM, Archibald L. FRIPP, Hu HUANG, and Kathy STACY
NASA Langley Research Center, Hampton, Virginia 23665
and
Richard T. SIMCHICK
Professional Research Corporation, Hampton, Virginia 23666

ABSTRACT

Direct visualization of the melt-solid interface during crystal growth in Bridgman furnaces will assist in controlling crystal composition and purity. Models of melt-solid interfaces have been radiographed, and methods of enhancing the images have been refined resulting in improved pictures of the position and shape of the interface in Lead Tin Telluride.

1. Introduction

In the melt growth of compound semiconductors, such as lead tin telluride (LTT) and mercury cadmium telluride (MCT), the shape of the melt-solid interface is recognized by theory as a factor in the determination of the composition and perfection of the final crystalline material.[1,2,3] In alloy semiconductors, in which there is crystallization from a mixture of two compounds such as lead telluride and tin telluride, one of the components is

preferentially excluded from the solid. The shape of the melt-solid interface affects this diffusion boundary layer and the subsequent incorporation of the excluded component. Consequently, the final compositional distribution is also affected. A uniform composition is important for the subsequent commercial use of these materials, since the band-gap of the resulting semiconductor is a function of this composition.[4,5,6]

Cracks and other mechanical flaws are believed to originate at the external heterogeneous interface between the semiconductor and the container wall. If the melt-solid interface is concave into the solid, then there exists a pool of molten material into which the solid with its flaws can grow. If the melt-solid interface is concave into the melt, i.e., if the solid has a convex shape, then there is no molten material into which cracks can grow. All such flaws are worked out of the material toward the container walls during growth.

The shape of melt-solid interfaces is regulated by surface tension, the temperature, and the composition profile across the sample in the furnace. The surface tension is determined principally by the materials being crystallized and the materials of the container or containment media. Surface tension is not an easily adjusted experimental parameter in the

Bridgman growth of a given semiconductor. The temperature profile, however, is an experimental variable accessible to the crystal grower. Temperature will alter the surface tension, but more significantly it causes the melt-solid interface to change position and shape.[7,8,9,10,11,12,13,14,15,16,17,18] Knowing what temperature profiles exist in a furnace and knowing what changes need to be made during growth to change the interface shape and location are important variables available to control the composition and perfection of crystals grown from the melt.

The use of visual light to directly view the melt-solid interface in semiconductors is not practical, since semiconductors have low Prandtl numbers and are opaque to visible light. Compounds and mixtures with high Prandtl numbers are transparent, but they are not semiconductors. The techniques that have been used to determine the interface position and shape have been available only after processing has been completed. One such technique is to grow the crystal in a given furnace with a known temperature profile, suddenly to quench the rest of the sample so as to freeze in the interface location and shape. The resulting boule is then cut, polished, and etched to reveal the interface. This was done with lead tin telluride and

germanium.[19,20] A second technique involves perturbing the composition of the growing crystal by periodically impressing mechanical or thermal shocks through vibrators and Peltier pulses. In this technique as well, the boule is cut open after processing, polished, and etched to reveal the interface locations and shapes. This was done in gallium doped germanium[21,22] and in indium antimonide.[23,24]

Although the existing post-processing techniques do reveal melt-solid interface locations and shapes and although they have demonstrated the experimental ability to change the interface shape, they do not allow the experimental observation and subsequent regulation of the interface locus and shape during actual crystal growth. There is a need for real-time visualization of interfaces during melt growth from furnaces such as Bridgman ones.

2. Interface Models

Visualizing the melt-solid interface in a dense material such as germanium, LTT, and MCT inside a steel lined ceramic Bridgman furnace requires the use of x-rays or gamma-rays. The radiographic techniques to do this have been developed and reported earlier in this journal.[25] These radiographic techniques have allowed the interface between the

melt and solid in LTT to be viewed. To improve the resulting image, standard methods of image enhancement have been used. Questions remain as to whether or not such procedures allow the shapes of melt-solid interfaces to be accurately determined and to what minimum density differences such techniques are capable of detecting interfaces. To answer these questions a series of models with known density differences and known interface shapes were constructed.

Metal templates were first fabricated with three known interface shapes from several aluminums and brasses. The interfaces selected were the following: one planar interface in a bar with a square cross-section and two curved interfaces in cylindrical rods. The two curved interfaces had radii equal to the radius of the cylinder and equal to twice that radius respectively. This resulted in the deep and shallow curved interfaces shown in figure 1. These metal models were so constructed as to be able to be interchanged end-for-end to provide three interface shapes in a variety of density differences. It was apparent from the first radiographs that the technique was sensitive enough always to reveal a small air gap between the rod ends. A series of models with more intimate contact were needed.

The metal models were used as templates to construct rubber molds into which epoxy resin (Shell 1132) was poured. The resin was made using only half the recommended hardener (Dow Chemical Hardener), and it was carefully degassed before pouring into the molds. When the undoped resin hardened, slightly doped resin was poured onto the interface. The resin was doped with five micrometer silicon carbide dust at four concentrations from 0.0625% to 0.5000% by weight. The resulting densities are summarized in Table 1.

TABLE 1: Densities of Doped and Undoped Epoxy Resin Interface Models

Doping Levels %SiC by weight	Measured Density g/cm^3	Relative X-Ray Density $\{n_{doped}/n_{undoped}\}$
0.500	1.2235	0.97
0.250	1.1993	0.98_4
0.125	1.1941	0.99_2
0.063	1.1896	0.99_6
0.000	1.12	1.00

The interfaces were now in intimate contact and radiographs were taken of these models. The geometry of the Bridgman furnace was duplicated as much as

possible. The film densities were made as similar to those used during the growth of actual semiconductors. The film densities were in the optimum range for the films, i.e., 1.5 to 2.0.

3. Image Enhancement

The resulting negatives were digitized using an Eikonix camera and subjected to the normal image enhancement techniques of linear stretching and smoothing to improve the contrast. This technique worked well with the radiographs of the planar interface models which have square cross-sections. Figure 2 illustrates that the planar interface could be accurately imaged down to the lowest doping level or a density difference of 0.02% across the interface.

There was a problem with the models of the curved interfaces on rods with circular cross-sections. Figure 3 is an enhanced image with contours, which illustrates that the samples with cylindrical geometry have a continual increase in film density from the center to the edge. This is caused by the continual reduction of path length through the material closer to the edges of the cylindrical models. Absorption of radiation is a function of both the density of the material and the amount of that material through which the radiation must pass.

This density difference caused by the geometry of the cylinders exceeds that difference due to the doping of the models. Enhancement using a simple linear stretch enables the planar interface on a square cross-section to be easily detected across the entire specimen. The same procedure applied to the cylindrical models only enables the interface to be detected in the central core or on the outer edges of the cylindrical sample. Stretching the intensities to make the doped-undoped interfaces visible in the core of the sample leaves the outer edge region too dark to distinguish the interface. Stretching the intensities to make the curved interface visible in these outer regions only makes the central core wash out. This cylindrical geometry is exactly the one existing in the Bridgman growth of semiconductors.

The image enhancement techniques of column averaging proved a suitable solution to this geometrical problem. This procedure was originally developed to aid in the interpretation of aerial photographs, for cylindrical geometry is characteristic of both imaging tasks. In this procedure the digitized image is oriented with its cylindrical axis vertical. Each vertical column is added across the entire image, and the total is displayed graphically. A least square quadratic line is fit to the resulting curve. The column averages

across one of the cylindrical models is displayed in figure 4. The distribution of intensities reflects the variation in sample width through which the radiation must pass. The least square quadratic equation is fit to the curve of the column sums. This quadratic equation is then used to scale the intensities across the cylindrical image. This scaled, corrected image is then subjected to the usual linear stretch to improve the contrast across the interface in the models. With the image corrected for cylindrical geometry, the entire interface is clearly visible in the image as illustrated in figure 5. The location and shape of the interface in the models, even in the ones with curved interfaces, were faithfully reproduced with the radiographic and image enhancement procedures.

4. Bridgman Grown Semiconductors

The techniques developed for the epoxy interface models were applied to radiographs taken with Ir^{192} gamma radiation through a Bridgman furnace and LTT sample. The resulting negatives were subjected to analysis using the column averaging correction described in this paper. Figure 6 has an example of the interface image obtained. The readers are invited to compare this figure with ones reported earlier in this journal.[25]

5. Conclusion

Using a column averaging image enhancement procedure together with standard linear stretching and smoothing routines on x-ray and gamma-ray radiographs significantly improves the resulting interface images even when these are obtained through 16mm of a very dense semiconductor such as LTT.

Procedures will be extended to obtain digitized radiographic images and to enhance them in real time.

6. Acknowledgement

One of the authors (P.G.B.) gratefully acknowledges the support received through NASA Grant NAG-1-627(4).

7. References

1 S.R. Coriell and R.F. Sekerka, J. Crystal Growth 46 (1979) 479-482.

2 F.R. Szofran and S.L. Lehoczky, J. Crystal Growth 70 (1984) 349-355.

3 K. Kinoshita and K. Sugii, J. Crystal Growth 71 (1985) 283-288.

4 P.W. Kruse, Semiconductors and Semimetals, vol 18 "Mercury Cadmium Telluride" (1981) 1-20.

5 S.G. Parker and R.E. Johnson, "Preparation and Properties of (Pb Sn) Te", vol. 6 (1981) 1-65.

6 A.L. Fripp and R.K. Crouch, Infrared Physics 19 (1979) 701-702.

7 C.E. Chang and W.R. Wilcox, J. Crystal Growth 21 (1974) 135-140.

8 Ta-Wei Fu and W.R. Wilcox, J. Crystal Growth 48 (1980) 416-424.

9 T. Jasinski and A.F. Witt, J. Crystal Growth 71 (1985) 295-304.

10 C.A. Wang, A.F. Witt, and J.R. Carruthers, J. Crystal Growth 66 (1984) 299-308.

11 F.M. Carlson, A.L. Fripp, and R.K. Crouch, J. Crystal Growth 68 (1984) 747-756.

12 F.M. Carlson, L-Y. Chin, A.L. Fripp, and R.K.

Crouch, "Materials Processing in the Reduced Gravity Environment of Space", 9 (1982) 629-649.

13 T.I. Ejim, W.A. Jesser, and A.L. Fripp, J. Crystal Growth 69 (1984) 509-514.

14 T.W. Clyne, J. Crystal Growth 50 (1980) 684-690.

15 C.E. Huang, D. Elwell, and R.S. Feigelson, J. Crystal Growth 64 (1983) 441-447.

16 P.M. Adornato and R.A. Brown J. Crystal Growth 80 (1987) 155-190.

17 C.J. Chang and R.A. Brown, J. Crystal Growth 63 (1983) 343-364.

18 C.L. Jones, P. Capper, J.J. Gosney, and I. Kenworthy, J. Crystal Growth 69 (1984) 281-290.

19 Y. Huang, W.J. Debnam, and A.L. Fripp, In preparation for J. Crystal Growth (1988).

20 P. Capper, J.J. Gosney, C.L. Jones, and M.J.T. Quelch, J. Crystal Growth 63 (1983) 154-164.

21 K.M. Kim and A.F. Witt, J. Electrochem. Soc. 125 (Mar 1978).

22 A.F. Witt, H.C. Gatos, M. Lichtensteiger, and C.J. Herman, J. Electrochem. Soc. 125 (Nov 1978) 1832-1840.

23 K.M. Kim, A.F. Witt, and H.C. Gatos, J. Electrochem. Soc. 119 (Sept 1972) 1218-1226.

24 D.E. Holmes and H.C. Gatos, J. Electrochem. Soc. 125 (Nov 1978) 1873-1875.

25 P.G. Barber, R.K. Crouch, A.L. Fripp, W.J. Debnam, R.F. Berry, and R. Simchick, J. Crystal Growth 74 (1986) 228-230.

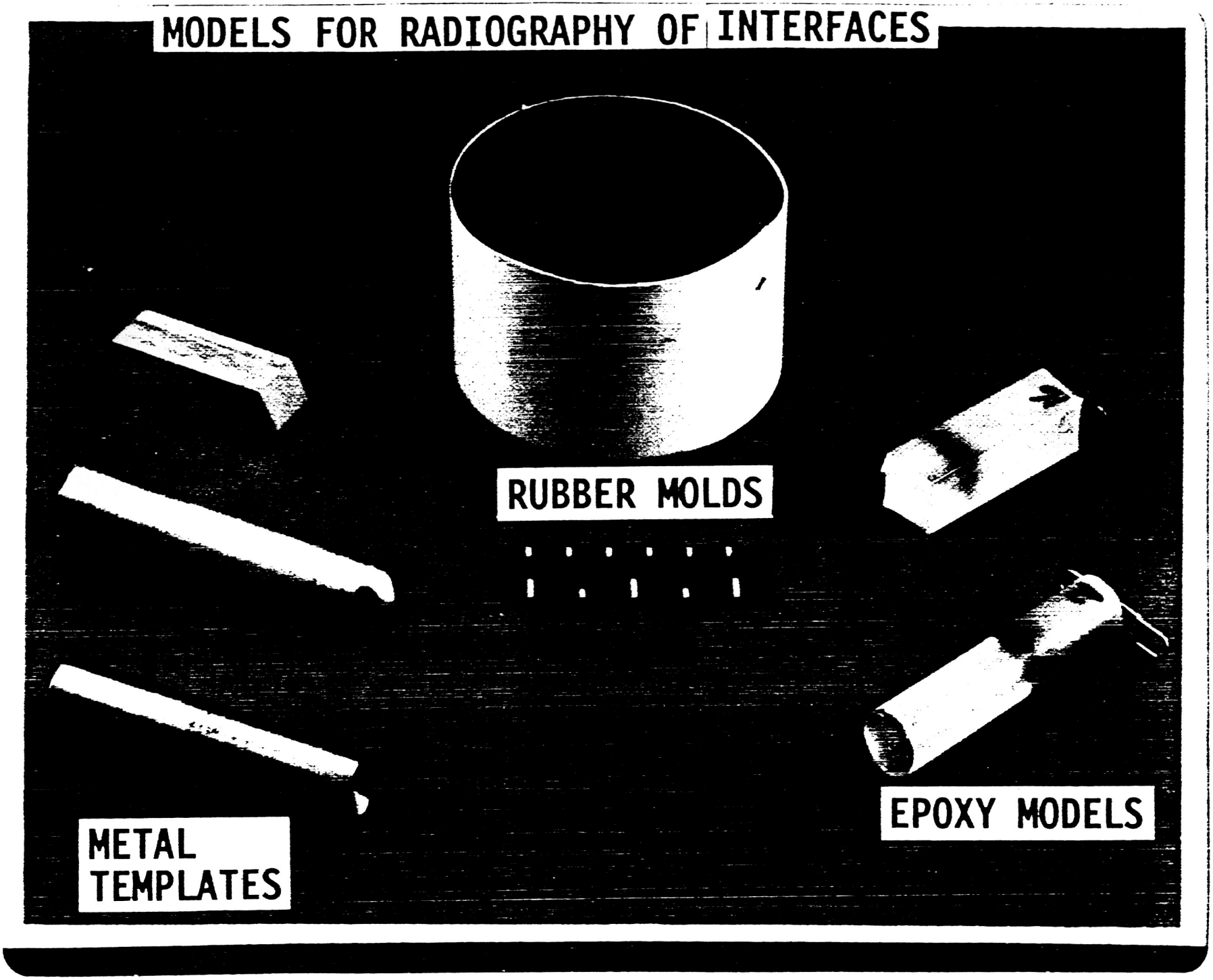

Figure 1: Models Used for Interface Radiography

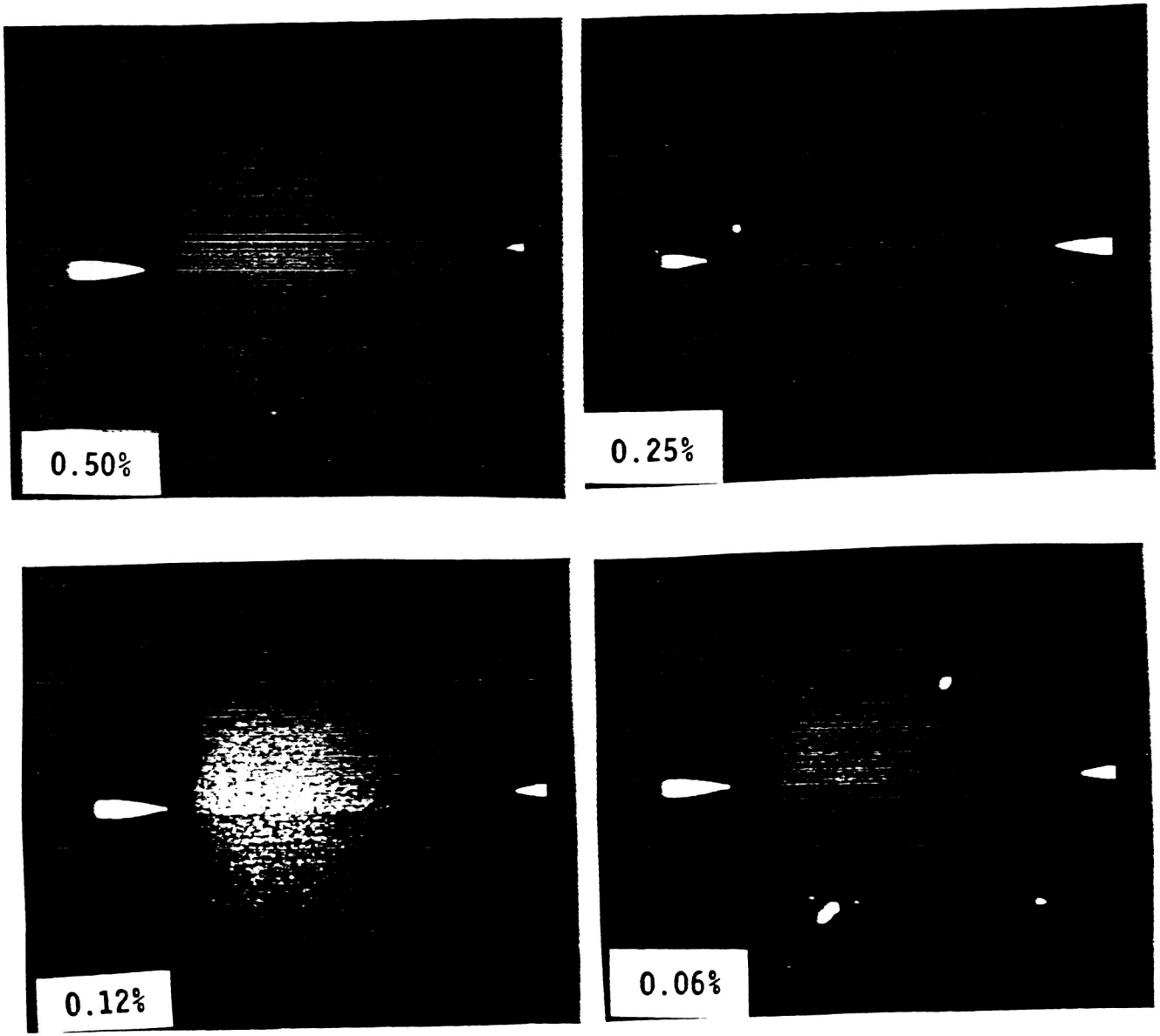

Figure 2: Enhanced Images of Planar Interfaces

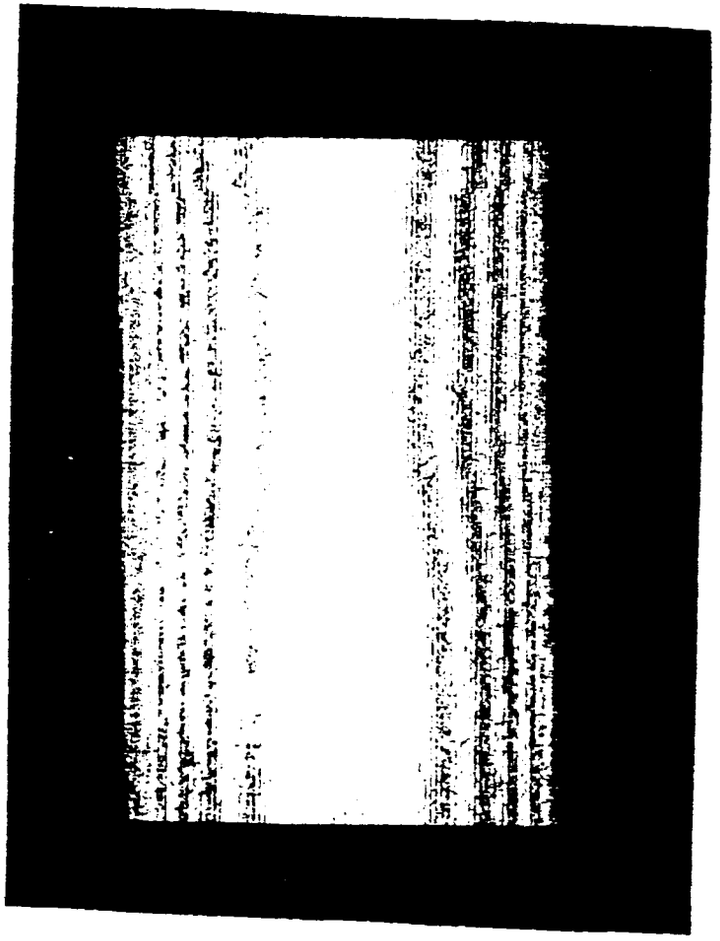

Figure 3: Contours Resulting from Cylindrical Sample Shape

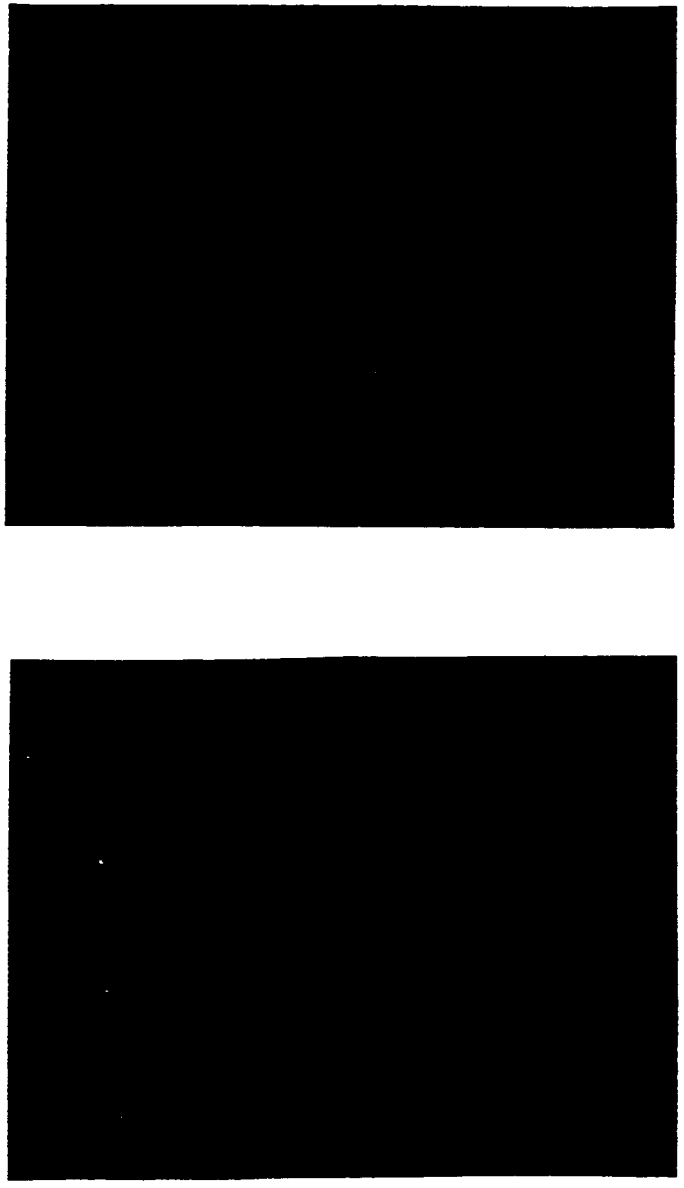

Figure 4: Curve-Fitting in Column Averaging

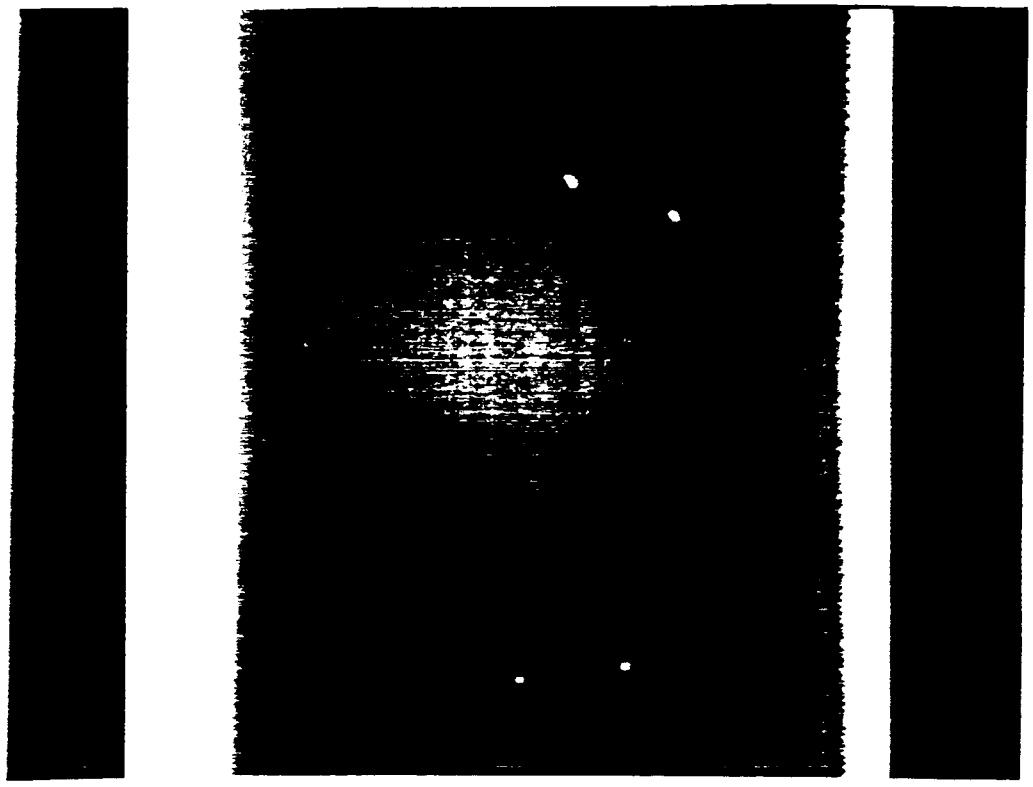

Figure 5: 0.50% SiC Epoxy Model with a Curved Interface

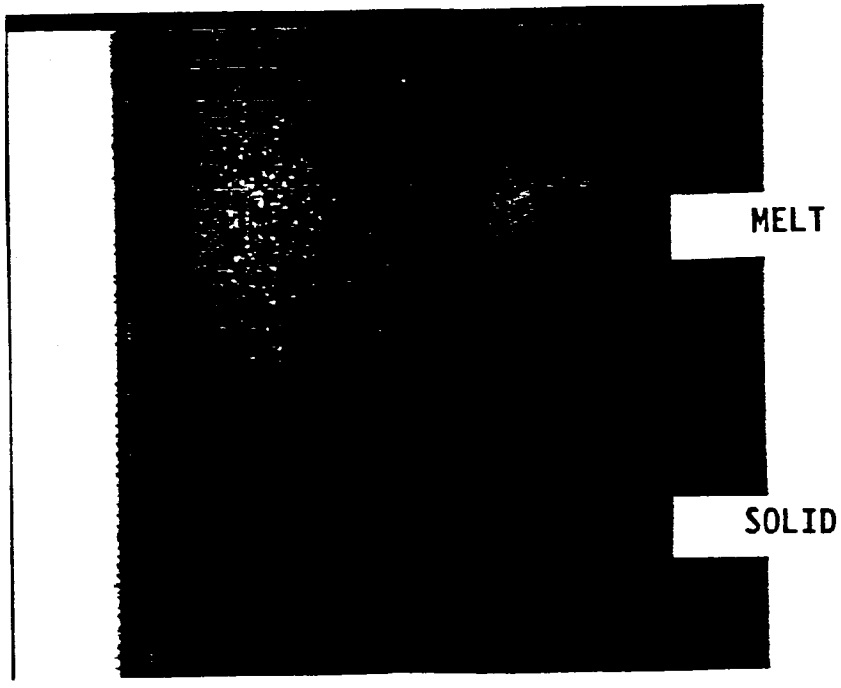

Figure 6: LTT Melt-Solid Interface Radiographed Through a Bridgman Furnace. Image has been corrected for cylindrical symmetry.